Available online at www.sciencedirect.com
SCIENCE DIRECT®
Chemical Physics Letters 365 (2002) 49–56
CHEMICAL PHYSICS LETTERS
www.elsevier.com/locate/cplett

Emission characteristics of CdS nanoparticles induced by confinement within MCM-41 nanotubes

Weon-Sik Chae, Ju-Hye Ko, In-Wook Hwang, Yong-Rok Kim *

Department of Chemistry, Yonsei University, 134 Schinchon-Dong, Seodaemun-Gu, Seoul 120-749, Republic of Korea

Received 18 March 2002; in final form 8 August 2002

Abstract

Nanosize CdS particles confined in siliceous MCM-41 channels were prepared by using reversed micelles as an insertion carrier. As-made CdS in MCM-41 host shows photoluminescence (PL) signals from both band-edge and surface defect state recombination. Calcinated CdS in the host, however, presents relatively suppressed surface defect state emission compared with band-edge emission. Such emission characteristics after calcination is ascribed to the reduced probability of recombination through deeply trapped surface defect states compared with direct excitonic recombination, which is possibly due to surface capping of the CdS nanoparticles by the host nanochannels.

1. Introduction

Nanosize semiconductors have attracted much interest in the fields of pure and interdisciplinary sciences for the last two decades due to their unique physical and chemical properties [1–3]. Among a variety of nanosize semiconductors, profitable merits such as band-gap energy in the visible region and an easy synthetic method make CdS the most extensively studied semiconductor [1,4]. Ultra-small CdS particles often present novel properties due to the quantum confinement effects of photo-excited carriers and the larger ratio of active surface atoms to bulk lattice atoms. There have been many studies on the preparation of CdS nanoparticles and the elucidation of their physical properties, such as absorption, emission, and optical phonon interactions [5–9]. Relaxation and transport properties of photo-excited carriers in the CdS nanostructures have also been extensively studied with simple or composite materials [10–14]. Nevertheless, the complicated optical properties of CdS semiconductor based systems still require further study.

Recently, structurally ordered arrays of CdS nanoparticles in long-range ordered mesoporous materials have been reported [15–18]. These studies were mainly focused on synthetic routes for novel semiconductor-based materials and their structural characterizations. Among them, the size selective incorporation of CdS within reversed micelles into surface modified MCM-41 was shown to be an efficient method for the preparation of ordered CdS nanostructures confined in

* Correspondence author. Fax: +82-2-364-7050.
E-mail address: yrkim@alchemy.yonsei.ac.kr (Y.-R. Kim).

0009-2614/02/$ - see front matter
PII: S0009-2614(02)01418-5

mesoporous hosts. Such a system was utilized for photo-catalytic hydrogen gas generation, although detailed information on the dynamics of photo-excited carriers and their energetics is not available [16]. Therefore, in this study, the optical properties of the nanosize CdS incorporated in the mesoporous MCM-41 nanochannels are discussed with respect to absorption, emission, and relaxation of the photo-excited carriers.

2. Experimental

2.1. Sample preparation

2.1.1. CdS nanoparticle in reversed micelle

Water containing sodium bis(2-ethylhexyl) sulfosuccinate (AOT, Aldrich) reversed micelles in an oil phase have often been used as a nanoreactor [19,20]. The water to AOT molecular ratio ($W_o = [H_2O]/[AOT]$) controls the size of the water pool in the reversed micelles. In this study, a W_o ratio of 2 was selected for the preparation of CdS nanoparticles. In order to prepare AOT/*n*-octane reversed micelles containing Cd^{2+} ions, 18 μl of 0.1 M $Cd(NO_3)$ aqueous solution was added to 5 ml AOT/*n*-octane (0.1 M) solution. On the other hand, the addition of 18 μl of 0.1 M Na_2S solution to 5 ml AOT/*n*-octane (0.1 M) solution resulted in AOT/*n*-octane reversed micellar solution containing S^{2-} ions. Mixing both the reversed micellar solutions produced nanosize CdS particles within the nanopools of the reversed micelles through rapid precipitation. The CdS nanoparticles in the reversed micelles were subsequently monitored using absorption measurements for 12 h in order to study the stability of the nanoparticle/reversed micellar system.

2.1.2. Surface modification of mesoporous host

A mesoporous MCM-41 host was prepared by utilizing a well-defined supramolecular templating method. The detailed procedures are described in a previous paper [21]. Since the surface of the mesoporous MCM-41 nanochannels is covered by hydrophilic silanol groups, insertion of reversed micelles containing CdS nanoparticles into such hydrophilic nanochannels is not an efficient process due to the hydrophobic surface of the reversed micelles. Therefore, in order to increase the insertion efficiency of the reversed micelles into the nanochannels of the mesoporous host, the surface silanol groups of the nanochannels were chemically modified as in a similar procedure of a reference [22]. The surface silanols of the MCM-41 nanochannels were modified by using tris(methoxy)mercaptopropylsilane (TMMPS) as an organic modification agent through covalent bonding linkage with silica wall framework, which resulted in the enhanced hydrophobicity of the nanochannels ($\equiv Si{-}CH_2CH_2CH_2SH$) [22]. The resulting TMMPS modified MCM-41 is denoted as ThMCM-41.

2.1.3. Insertion of CdS nanoparticles into mesoporous host

Insertion of the CdS nanoparticle/AOT/*n*-octane reversed micelles into the nanochannels of a finite size host was conducted according to the following procedure: 0.3 g of ThMCM-41 was added to the CdS/AOT/*n*-octane reversed micellar solution after formation of CdS nanoparticles (ca. 5 min). The mixture was slowly stirred for 12 h to insert the CdS reversed micelles into the ThMCM-41 nanochannels. The final solution was centrifuged and the supernatant solution was then measured for absorption to estimate the insertion amount [16]. The isolated powder was dried overnight in an oven at 97 °C. Since the organic molecules of the AOT surfactant, the TMMPS, and the residual *n*-octane might modify recombination processes of photo-generated carriers, the organic molecules were removed by calcination in a furnace at 500 °C for 2 h after insertion. The CdS confined in the nanochannels of MCM-41 is denoted as CdS@MCM-41.

2.2. Characterization

Absorption spectra of the CdS/AOT/*n*-octane reversed micelles were measured with a UV–Vis spectrophotometer (Shimadzu, UV-160A). The size of CdS nanoparticles was estimated from the UV–Vis absorption spectra by utilizing the quantum size effect [3,4]. To prove the organic modification of the MCM-41 channel surface, infrared

spectra were measured with a FT-IR spectrophotometer (Perkin–Elmer, Spectrum BX FT-IR), and thermogravimetric analysis (TGA) and differential weight loss (DTG) were also conducted, as a function of temperature, on a thermogravimetric analyzer (TA Instruments, TA2050) with a scan speed of 10 °C/min under Ar flow. Transmission electron microscopy (TEM) imaging was obtained with a TEM (Philips, CM-20) that was operated at 200 kV with the sample deposited on a holey carbon copper grid. For the powder type of CdS@MCM-41, diffuse reflectance spectra were recorded on a UV–Vis spectrophotometer (Shimadzu, UV3101PC) equipped with an integrating sphere (Shimadzu, ISR-2200). Photoluminescence (PL) spectra were obtained by using a fluorimeter (Hitachi, F-4500). A picosecond time-correlated single photon counting (TCSPC) system was employed for the measurement of time-resolved PL decay. Details of the laser system and lifetime fitting method were described in Refs. [23,24]. The PL and PL lifetime measurements were performed under the same experimental conditions for all powdered samples in quartz cuvette (10 mm × 1 mm).

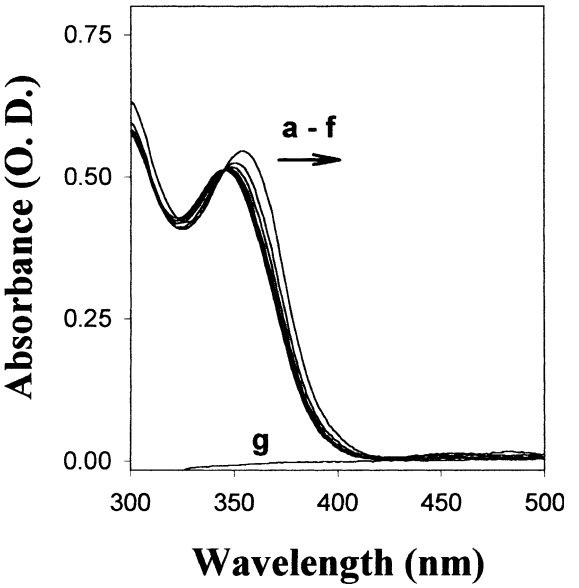

Fig. 1. Spectral shift of the absorption spectrum for the nanosize CdS in the reversed micelles ($W_o = 2$) observed for 12 h: (a) as-made, (b) 10 min, (c) 30 min, (d) 1 h, (e) 2 h, (f) 12 h, and (g) absorption spectrum of the supernatant solution after insertion process of 12 h.

3. Results and discussion

After formation of the CdS nanoparticles within the water pool of reversed micelles, its lowest electronic absorption (exciton absorption) peak is gradually red-shifted during the observation period of 12 h [Fig. 1], which indicates that the size of as-made CdS particles becomes slightly larger [2–4]. The size of CdS nanoparticles in this Letter was estimated by utilizing a modified effective mass approximation (MEMA), which was proposed by Nosaka in a previous report [25]. Since the MEMA did not consider the polarization term in nanodomain, the MEMA could somewhat underestimate the real particle size within a few angstrom. Nevertheless, the previous report indicated that the estimated size of semiconductor nanoparticles by the MEMA was reasonably comparable to the reported particle size from X-ray diffraction as elsewhere reported [25]. From the electronic absorption spectra of the CdS nanoparticles within the water pool of reversed micelles [Fig. 1a–f], the estimated size by the MEMA indicates that the particle size is slightly increased from 1.6 to 1.7 nm in diameter over 12 h.

Surface modification of the mesoporous MCM-41 was confirmed by characteristic vibrational modes (2580 cm^{-1} and 2900–3000 cm^{-1} corresponding to thiol groups and hydrocarbons of the modification agent, respectively, as elsewhere reported [17]) and by thermal weight loss at the ~360 °C region, which corresponds to the weight loss of modified organic part of the ThMCM-41 (data not shown here).

For the ThMCM-41 host, the TEM image clearly shows a hexagonal honeycomb structure [Fig. 2a]. After insertion of the reversed micelles containing CdS nanoparticles into the ThMCM-41 nanochannels, an absorption peak for the CdS nanoparticles is not observed from the supernatant solution [Fig. 1g]. This suggests that the CdS nanoparticles (1.6–1.7 nm)/reversed AOT micelles in solution were completely inserted into the nanochannels of the mesoporous host (channel

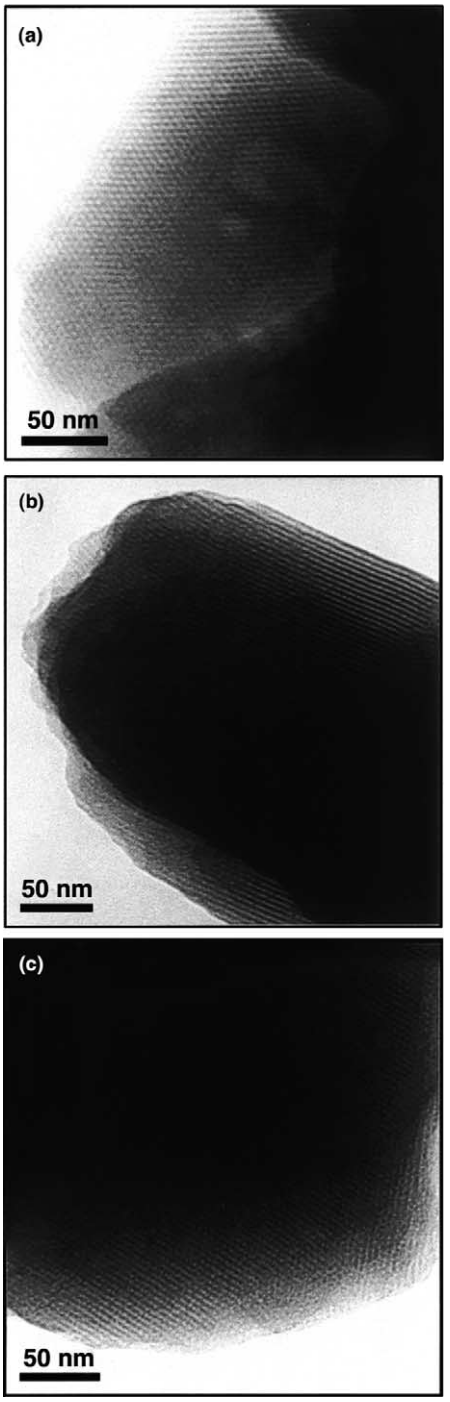

Fig. 2. TEM images for (a) ThMCM-41 at a pore opening direction (hexagonal), (b) as-made CdS@MCM-41 at a perpendicular direction to the pore opening (lamellar), and (c) calcinated CdS@MCM-41 (lamellar).

diameter of ~3 nm from TEM image). Even after insertion of the CdS reversed micelles into the ThMCM-41 nanochannels, long-range ordered channel structure is well conserved for the as-made CdS@MCM-41 [Fig. 2b] and also for the calcinated CdS@MCM-41 [Fig. 2c]. However, the CdS nanoparticles within the host channel are not well resolved from the TEM image contrast of the channel and the wall structure of the host. This is possibly due to the low electron density of small CdS nanoparticles compared with the massive mesoporous host [17]. Existence of the CdS nanoparticles within the nanochannels of the host, however, can be proved by absorption and emission spectra.

Diffuse reflectance spectrum for the ThMCM-41 shows steep absorption at ~310 nm, which is attributed to the organic part of the ThMCM-41 [Fig. 3a]. For the as-made CdS@MCM-41, extended absorption to ~450 nm (~2.8 eV) is additionally observed [Fig. 3a]. This extended broad absorption band is possibly due to the band-gap absorption of CdS nanoparticles. Such blue-shifted absorption compared with the reported value of band-gap absorption (2.5 eV [7]) for bulk CdS is believed to be due to the quantum confinement effect that is observed as photo-excited electron and hole pair (exciton) is confined in a nanoscaled domain less than the Bohr radius of the exciton [2–4]. However, discrete exciton absorption that is observed in the CdS/reversed micellar system does not appear in the as-made CdS@MCM-41. Such a broad absorption feature is possibly caused from broad distribution of exciton states due to particle sizes and/or shape distribution of the CdS within the nanochannels. Although exact particle size is difficult to be estimated from such broad absorption spectra, the upper limit (~3.0 nm) of the CdS particle size, which was estimated from absorption onset (~450 nm) of the as-made CdS@MCM-41, implies that the CdS particles in the reversed micelles grew in the nanochannels after insertion. Furthermore, it is noticeable that the size of the CdS particles within the MCM-41 host does not exceed the channel diameter of the host (~3 nm). After calcination of the as-made CdS@MCM-41, absorption spectrum exhibits a shoulder at ~400 nm as well as the extended absorption edge to

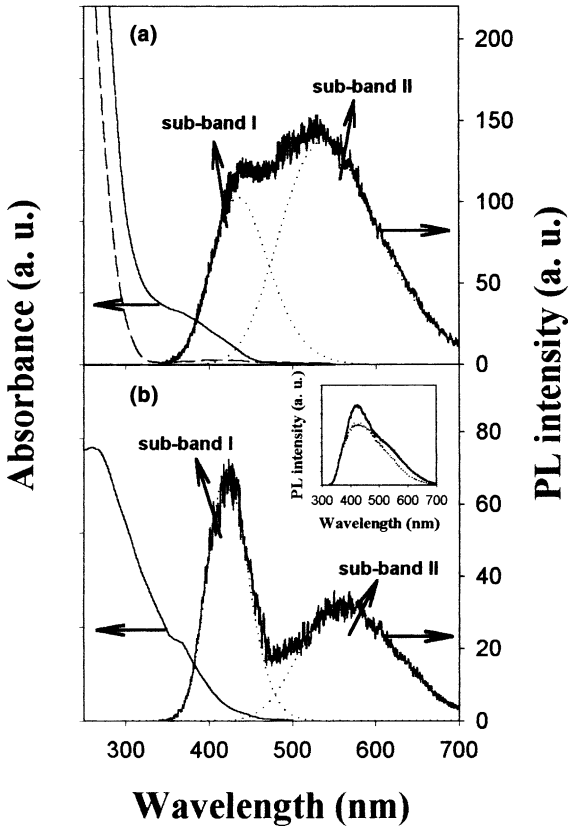

Fig. 3. Diffuse reflectance and PL spectra (solid line) for (a) as-made CdS@MCM-41 and (b) calcinated CdS@MCM-41 at room temperature. The diffuse reflectance spectrum for ThMCM-41 (dashed line) is also presented. The PL spectra are fitted by two sub-Gaussian bands (dotted line). Inset: PL spectra for calcinated host itself (dotted line) and calcinated CdS@MCM-41 before subtraction of the host emission (solid line) at room temperature. Excitation wavelength for all PL spectra is 340 nm.

~450 nm, from which it is considered that the size of the CdS nanoparticles is partially reduced from the size of the as-made CdS@MCM-41 after calcination [Fig. 3].

The as-made CdS@MCM-41 exhibits two broad emission peaks centered at 430 (sub-band I) and 530 nm (sub-band II) [Fig. 3a]. According to previous reports [26–29], such band-edge emission (sub-band I) is ascribed to excitonic recombination, and the largely Stokes shifted emission (sub-band II) is due to surface defect states such as sulfur vacancies and/or sulfur dangling bonds. After calcination of the CdS@MCM-41, defect states are also generated in the calcinated siliceous host itself [inset of Fig. 3b]. Thus the emission induced by the host defects is subtracted from the PL spectrum of the calcinated CdS@MCM-41, which results in two emission bands centered at 420 (sub-band I) and 560 nm (sub-band II) for the CdS nanoparticles [Fig. 3b]. It is interesting that the sub-band I shows relatively higher emission intensity than the sub-band II after calcination. Based on the PL results, such emission characteristics after calcination can be explained by the following two main factors. One is the increased probability of the direct electron and hole (exciton) recombination caused by increased interaction probability between the photo-excited electron and the hole wavefunctions. Such increased electron–hole interaction possibly occurs due to the size reduction of the CdS nanoparticle after heat treatment. The other is the suppressed surface state emission caused by decreased probability of nonradiative trapping of the photo-excited electrons in the conduction band (CB) and/or the shallow trapped (ST) state by broad surface defect states. Such reduction of trapping probability of the photo-excited electrons decreases recombination through the surface defect states. For the calcinated CdS@MCM-41, the trapping probability of the photo-excited electrons is possibly reduced by partial capping of the CdS nanoparticles with the nanochannels of the host since the surface capping reduces the number of surface defect sites located at the surface of the CdS nanoparticle.

Time-resolved PL decays for both before and after calcination of the CdS@MCM-41 are presented in Fig. 4. For the as-made CdS@MCM-41, fast (~0.1 ns) and slow (5–13 ns) lifetime components are observed. After calcination of the CdS@MCM-41, the fast (~0.2 ns) and the slow (10–11 ns) lifetime components are still observed. Lifetime amplitude profiles imply that the fast and the slow lifetime components are mainly responsible for the band-edge emission (sub-band I) and the largely Stokes shifted emission (sub-band II), respectively [Table 1]. Therefore, it is considered that the fast lifetime component is related to the excitonic recombination process, and the slow

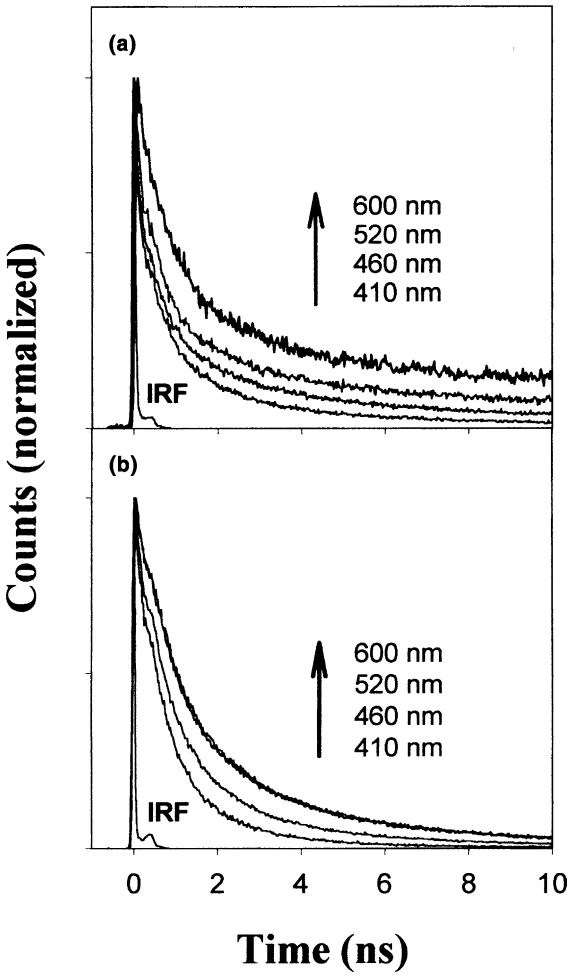

Fig. 4. Time-resolved PL decays for (a) as-made CdS@MCM-41 and (b) calcinated CdS@MCM-41 as a function of detection wavelength at room temperature. Instrumental response function (IRF) is 67 ps (full width at half maximum). Excitation wavelength for the PL decays is 293 nm.

lifetime component is related to the recombination process through the surface defect states. Furthermore, it is noticeable that the lifetime of the fast component changes from ~0.1 ns in the as-made CdS@MCM-41 to ~0.2 ns in the calcinated CdS@MCM-41 and, also, the slow lifetime component (5–13 ns) for the as-made CdS@MCM-41 shows relatively wider lifetime distribution and higher lifetime amplitude contribution (%) than the slow lifetime component (10–11 ns) for the calcinated CdS@MCM-41 [Table 1]. Generally, PL lifetime depends on the rates of radiative and nonradiative decays of photo-excited electrons in the CB state and/or the ST state. In the case of nanoscaled semiconductors, nonradiative trapping of the photo-excited electrons within the potential well of surface defect states usually occurs in a fast timescale (10^{-11}–10^{-14} s) [30–32], whereas the radiative recombination of the electrons in the CB state and/or the ST state and the holes in the valence band and/or the trap state occurs in a timescale of several hundred picoseconds to several nanoseconds [12,32,33]. Therefore, the lengthened PL lifetime of the fast excitonic emission (sub-band I) in the calcinated CdS@MCM-41 implies that the direct radiative recombination path of the photo-excited electrons and the holes relatively increases while the fast nonradiative trapping decreases, which is consistent with the reduced amplitude contribution (%) of the slow lifetime component [Table 1] and the discussion for the steady-state PL emissions [Fig. 3] after calcination. Furthermore, it is generally expected that the radiative recombination lifetime of exciton decreases as particle size decreases, due to increased interaction probability between the electron and the hole wavefunctions confined in reduced particle size, as indicated in a previous paper [10]. For the calcinated CdS@MCM-41, although the particle size is partially reduced as discussed in the absorption spectrum, the fast excitonic recombination lifetime is lengthened. Therefore, it is considered that the observed emission characteristics is not mainly responsible for the reduced particle size, but possibly for the surface capping of the CdS nanoparticles by nanochannels of the host.

The recombination rate from the surface defect states (sub-band II) is believed to be related to the recombination process of the distant pairs (trapped electron and hole pairs) [10,12]. Therefore, the broad distribution of the slow lifetime component (5–13 ns) reflects that the distant pairs have broad distribution of their distances in the as-made CdS@MCM-41. However, narrow distribution of the slow PL lifetime component (10–11 ns) is observed for the calcinated CdS@MCM-41, from which it is considered that the distance distribution of trapped electron and hole pairs becomes rela-

Table 1
Photoluminescence (PL) decay lifetimes for the CdS nanoparticles encapsulated in the MCM-41 nanochannels

Sample	λ_{em} (nm)	τ_1 (ns)	τ_2 (ns)	χ^2
As-made CdS@MCM-41	410	0.09 (91.9%)	5.06 (8.1%)	1.4
	460	0.11 (85.5%)	6.82 (14.5%)	1.4
	520	0.12 (76.8%)	10.60 (23.2%)	1.5
	600		12.50 (100.0%)	1.4
Calcinated CdS@MCM-41[a]	410	0.20 (99.4%)	10.00 (0.6%)	1.3
	460	0.20 (95.8%)	10.17 (4.2%)	1.1
	520	0.21 (86.9%)	10.37 (13.1%)	1.2
	600		10.80 (100.0%)	1.3

$I(t) = A_1 e^{-t/\tau_1} + A_2 e^{-t/\tau_2}$; $I(t)$ is the time-dependent PL intensity, A is the amplitude (noted as the normalized percentage in the parenthesis), and τ is the lifetime. The excitation wavelength is 293 nm. λ_{em} represents the detection wavelength for the PL lifetime measurement.

[a] For the calcinated CdS@MCM-41, additional lifetime components of 0.9 and 2.6 ns are observed, which are originated from the possible defects existing in the calcinated host itself. Only the lifetime components of the CdS nanoparticles are presented for comparative study with the as-made CdS@MCM-41.

tively more homogeneous after removal of the organic moieties in the CdS@MCM-41 composite. From such results, the distribution of pair distances is supposed to be possibly influenced by organic moieties existing in its interface.

4. Conclusions

CdS nanoparticles were successfully incorporated into mesoporous MCM-41 nanochannels by using reversed micelles as an insertion carrier. The as-made CdS@MCM-41 exhibits band-edge emission as well as surface defects induced emission. However, the calcinated CdS@MCM-41 exhibits more intense band-edge emission compared with the emission from the surface defect states. The PL lifetime of the fast component becomes longer, from ~0.1 ns in the as-made CdS@MCM-41 to ~0.2 ns in the calcinated CdS@MCM-41. This slowed PL lifetime indicates that direct excitonic recombination is more probable than trapping to the surface defect states after the calcination of the CdS@MCM-41. Such emission properties are possibly induced from the surface capping of the CdS nanoparticles by the nanochannels of the mesoporous host. Moreover, it is suggested that the calcinated CdS@MCM-41 has more homogeneous distance distribution of the trapped electron and hole pairs than the as-made CdS@MCM-41.

Acknowledgements

This work has been financially supported by Grant No. 1999-2-121-004-5 from the interdisciplinary research program of the KOSEF. We are grateful for instrumental support from the equipment facility of CRM-KOSEF, Korea University.

References

[1] G.D. Stucky, J.E. MacDougall, Science 247 (1990) 669.
[2] A.P. Alivisatos, Science 271 (1996) 933.
[3] A.P. Alivisatos, J. Phys. Chem. 100 (1996) 13226.
[4] Y. Wang, N. Herron, J. Phys. Chem. 95 (1991) 525.
[5] J.J. Ramsden, M. Grätzel, J. Chem. Soc. Faraday Trans. 1 (80) (1984) 919.
[6] R. Rossetti, J.L. Ellison, J.M. Gibson, L.E. Brus, J. Chem. Phys. 80 (1984) 4464.
[7] R. Rossetti, R. Hull, J.M. Gibson, L.E. Brus, J. Chem. Phys. 82 (1985) 552.
[8] Y. Wang, N. Herron, Phys. Rev. B 42 (1990) 7253.
[9] J.J. Shiang, S.H. Risbud, A.P. Alivisatos, J. Chem. Phys. 98 (1993) 8432.
[10] N. Chestnoy, T.D. Harris, R. Hull, L.E. Brus, J. Phys. Chem. 90 (1986) 3393.
[11] N. Herron, Y. Wang, H. Eckert, J. Am. Chem. Soc. 112 (1990) 1322.

[12] M. O'Neil, J. Marohn, G. McLendon, J. Phys. Chem. 94 (1990) 4356.
[13] A. Hässelbarth, A. Eychmüller, R. Eichberger, M. Giersig, A. Mews, H. Weller, J. Phys. Chem. 97 (1993) 5333.
[14] S. Logunov, T. Green, S. Marguet, M.A. El-Sayed, J. Phys. Chem. A 102 (1998) 5652.
[15] W. Chen, Y. Xu, Z. Lin, Z. Wang, L. Lin, Solid State Commun. 105 (1998) 129.
[16] T. Hirai, H. Okubo, I. Komasawa, J. Phys. Chem. B 103 (1999) 4228.
[17] H. Wellmann, J. Rathousky, M. Wark, A. Zukal, G. Schulz-Ekloff, Micropor. Mesopor. Mater. 44–45 (2001) 419.
[18] Z. Zhang, S. Dai, X. Fan, D.A. Blom, S.J. Pennycook, Y. Wei, J. Phys. Chem. B 105 (2001) 6755.
[19] G.C. De, A.M. Roy, S. Saha, J. Photochem. Photobiol. A 92 (1995) 189.
[20] P. Calandra, M. Goffredi, T. Liveri, Colloids Surf. A 160 (1999) 9.
[21] J.-S. Jung, W.-S. Chae, R.A. McIntyre, C.T. Seip, J.B. Wiley, C.J. O'Connor, Mater. Res. Bull. 34 (1999) 1353.
[22] M. Park, S. Komarneni, Micropor. Mesopor. Mater. 25 (1998) 75.
[23] I.-W. Hwang, H.-H. Choi, B.-K. Cho, M. Lee, Y.-R. Kim, Chem. Phys. Lett. 325 (2000) 219.
[24] W.-S. Chae, I.-W. Hwang, J.-S. Jung, Y.-R. Kim, Chem. Phys. Lett. 341 (2001) 279.
[25] Y. Nosaka, J. Phys. Chem. 95 (1991) 5054.
[26] L. Spanhel, M. Hasse, H. Weller, A. Henglein, J. Am. Chem. Soc. 109 (1987) 5649.
[27] Y. Wang, A. Suna, J. McHugh, E.F. Hilinski, P.A. Lucas, R.D. Johnson, J. Chem. Phys. 92 (1990) 6927.
[28] T. Dannhauser, M. O'Neil, K. Johansson, D. Whitten, G. McLendon, J. Phys. Chem. 90 (1986) 6074.
[29] A.R. Kortan, R. Hull, R.L. Opila, M.G. Bawendi, M.L. Steigerwald, P.J. Carroll, L.E. Brus, J. Am. Chem. Soc. 112 (1990) 1327.
[30] M. Kaschke, N.P. Ernsting, H. Weller, U. Muller, Chem. Phys. Lett. 168 (1990) 543.
[31] N.P. Ernsting, M. Kaschke, H. Weller, L. Katsikas, J. Opt. Soc. Am. B 7 (1990) 1630.
[32] G. Ghislotti, D. Ielmini, E. Riedo, M. Martinelli, M. Dellagiovanna, Solid State Commun. 111 (1999) 211.
[33] H. Gotoh, H. Ando, T. Takagahara, J. Appl. Phys. 81 (1997) 1785.